How to improve efficiency and robustness of the Newton method in geometrically non-linear structural problem discretized via displacement-based finite elements

Domenico Magisano[a,*], Leonardo Leonetti[a], Giovanni Garcea[a]

[a] *Dipartimento di Ingegneria Informatica, Modellistica, Elettronica e Sistemistica Università della Calabria 87036 Rende (Cosenza), Italy*

Abstract

In this paper we show how to significantly improve the robustness and the efficiency of the Newton method in geometrically non-linear structural problems discretized via displacement-based finite elements. The strategy is based on the relaxation of the constitutive equations at each integration point. This leads to an improved iterative scheme which requires a very low number of iterations to converge and can withstand large steps in step-by-step analyses. The computational cost of each iteration is the same as the original Newton method. The impressive readier convergence of the proposal is shown by many numerical tests. In geometrically non-linear analysis, the proposed strategy, called MIP Newton, is destined to replace the standard Newton method in any finite element code based on displacement formulations. Its implementation in existing code is very easy.

Keywords: Geometric non-linearities, finite deformation, step-by-step, displacement FE, integration points, MIP Newton.

*Corresponding author

Email addresses: domenico.magisano@hotmail.it (Domenico Magisano), leonardo.leonetti@hotmail.it (Leonardo Leonetti), giovanni.garcea@unical.it (Giovanni Garcea)

URL: www.labmec.unical.it (Giovanni Garcea)

1. Introduction

Slender structures are usually characterized by large displacements and rotations but small strains. This situation is commonly known as finite deformation or geometrically non-linear problem, that is a mathematical problem in which the non-linearities are due to geometric effects, that is the non-linear relationship between the strains and the displacements/rotations. Many practical problems can be framed in this context. Some examples are metal [1, 2, 3] and composite structures [4, 5, 6], often characterized by buckling phenomena and strong imperfection sensitivity [7, 8, 9], drape simulation problems [10, 11] and deployable structures [12] characterized by very large displacements.

The standard approach to simulate the behavior of this kind of structure consists of the use of the finite element (FE) method, in order to transform the continuum problem into a discrete one. The non-linear discrete equations, completed with an arc-length constraint defining the step size, are solved step-by-step by using the Newton iterative method, in order to evaluate the equilibrium path of the structure.

Although this strategy is well-established, it is plagued by its high computational cost, due to two different limitations: i) the number of FE degrees of freedom (DOFs) used to approximate the differential equations; ii) the number of iterations required to obtain an equilibrium point and then to trace the desired equilibrium path, once the continuum problem has been discretized. In this work attention is focused only on the second aspect and, to avoid any misunderstandings, we clarify that the word "convergence", used throughout the paper, refers only to the iterative method, which provides the solution of the non-linear discrete problem.

Most of the existing FE codes are based on displacement formulations, i.e. the kinematic field is interpolated and the discrete kinematic DOFs represent the unknowns of the non-linear equations. Other kinds of formulations are possible, like for instance the mixed (stress-displacement) one, also known as hybrid-stress, in which both the stress and the displacement fields are interpo-

lated. When comparing mixed and displacement finite elements many authors observe that the mixed ones are more robust and allow larger steps in path-following geometrically non-linear analyses [13, 14, 15]. This phenomenon was investigated for the first time some years ago in [16], when it was shown that the robustness and the efficiency (in terms of number of iterations) of the Newton iterative scheme are penalized in displacement formulations because of a phenomenon that was called "extrapolation locking". This is not a locking of the FE discretization, but of the iterative scheme usually found in beam/shell problems, when the axial/membranal stiffness is much higher than the flexural one. In these cases the iteration matrix evaluated in the current estimates of the equilibrium point can be far from the optimal one, in terms of the convergence condition of the Newton method. The number of iterations required to evaluate the equilibrium path, quickly grows as the stiffness ratios of the structure increase while, at the same time, the step size required to avoid loss of convergence drastically decreases. This phenomenon, that is typical of FE displacement formulation, does not affect mixed FE formulations, which are free from "extrapolation locking" [17, 18, 19]. In recent years many other researchers have experienced the better behavior of the mixed FE models in geometrically non–linear analyses. In [14] a displacement and a mixed (hybrid-stress) solid-shell FE are developed which, if converged, yield close predictions. However, the authors conclude that the mixed element converges more readily and can withstand larger load increments than the displacement one in all the examined problems. In [13], the author draws similar conclusions in the context of standard shell FEs. In the ABAQUS manual (29.3.3-9) [20] it is reported that hybrid beam elements are provided in order to make the convergence of the iterative method faster, when the beam's rotations are large. A recent work [21] investigated the fast convergence and the high robustness of mixed FE models, providing a clear explanation of the origin of the phenomenon in a general context. It was shown that the evolution of the displacement iterative process is forced to satisfy the constitutive equations at each iteration and this constraint leads to a deterioration in the convergence properties. On the contrary

in mixed FE models the stress DOFs are primal variables, directly extrapolated and corrected, which only at convergence satisfy the discrete constitutive equations. The mixed iterative scheme is then free to naturally evolve to the solution while the displacement iterative scheme is constrained to follow an assigned evolution in which the constitutive equations must be satisfied. Thus, the ready convergence of the Newton method for mixed FEs is not linked to the FE interpolation, but due to the different "format" of the iterations. Mixed elements have a higher computational cost in constructing their element stiffness matrix and internal force vector with respect to displacement FEs, because of the stress extra-variables usually condensed at element level, but their use in geometrically non-linear problems is justified by their readier convergence.

The question posed in this paper is *"Is it possible to use a mixed iterative scheme without introducing a mixed FE interpolation?"*. A positive answer to this question would have important implications since a great part of the existing code is based on well-established displacement FE interpolations. In this paper we will show that this is possible and a mixed format of the Newton method for geometrically non-linear structural problems discretized via displacement-based finite elements is presented. The strategy is inspired by the more efficient iterative scheme for mixed FE models. The idea consists of the relaxation of the constitutive equations at each integration point. In this way, the stiffness matrix of a displacement-based FE maintains its original form. The only difference is that the stresses at each integration point, used for the matrix evaluation, are directly extrapolated and corrected, i.e. used as primal variables. This leads to a "better" iteration matrix, which allows a very low number of iterations and very large steps (load increments) in step-by-step analyses. With respect to mixed FEs no stress interpolations are present, so avoiding any additional cost in the evaluation of the stiffness matrix. Furthermore the final equilibrium path is the same as the original displacement formulation since the constitutive law is recovered exactly at convergence.

The method, that we call MIP (Mixed Integration Point) Newton, converges much faster than the standard Newton method, as shown by many numerical

tests with different structural models and FEs. The gain in terms of number of iterations required is impressive as well as the very large steps (load increment) that the MIP Newton can withstand without loss of convergence. The computational cost of a MIP iteration is the same as a standard one. Furthermore, the iteration matrix evaluated with the MIP strategy is so "good" that the modified version of the method (MIP modified Newton), which computes and decomposes the iteration matrix at the first estimate of each equilibrium point, can be conveniently adopted. From the implementation point of view, a few changes to the standard approaches are required, without upsetting the existing FE codes and then its inclusion is straightforward. In geometrically non-linear analysis, the proposed strategy is so robust, efficient and simple that it is destined to replace the standard Newton method in any finite element code based on displacement formulations.

The paper is organized as follows: Section 2 presents a short overview of the Newton method in step-by-step analyses and the equations of a general displacement-based finite element, in order to introduce the notation; Section 3 derives the new MIP Newton in both the full and modified version; Section 4 presents the two structural models and their FE interpolations used in the numerical tests together with some implementation details required to make the numerical tests reproducible; Section 5 presents a series of numerical tests and discusses the improvements in terms of robustness and efficiency of the proposal; finally the conclusions are reported in Section 6.

2. Step-by-step geometrically non-linear analysis via displacement FEs

2.1. The discrete non-linear equations

We consider a slender hyperelastic structure subject to conservative loads $p[\lambda]$ proportionally increasing with the amplifier factor λ. The equilibrium is expressed by the virtual work equation

$$\Phi[u]'\,\delta u - \lambda p\,\delta u = 0 \quad , \quad u \in \mathcal{U}\ ,\ \delta u \in \mathcal{T} \tag{1}$$

where $u \in \mathcal{U}$ is the field of configuration variables, $\Phi[u]$ denotes the strain energy, $\mathcal{T}$ is the tangent space of $\mathcal{U}$ at u and a prime is used to express the Fréchet derivative with respect to u. We assume that $\mathcal{U}$ will be a linear manifold so that its tangent space $\mathcal{T}$ will be independent of u. In displacement formulation u is the displacement field, while when a mixed formulation is adopted u collects both displacement and stress fields. Eq.(1) can be rewritten, using a FE discretization $u = \mathbf{N}_u \mathbf{u}$ as

$$\mathbf{r}[\mathbf{u},\, \lambda] \equiv \mathbf{s}[\mathbf{u}] - \lambda\, \mathbf{p} = \mathbf{0}, \quad \text{with} \quad \begin{cases} \mathbf{s}^T \delta\mathbf{u} \equiv \Phi'[u]\delta u \\ \mathbf{p}^T \delta\mathbf{u} \equiv p\, \delta u \end{cases} \tag{2}$$

where $\mathbf{r} : \mathbb{R}^{N+1} \to \mathbb{R}^N$ is a non-linear vectorial function of the vector $\mathbf{z} \equiv \{\mathbf{u}, \lambda\} \in \mathbb{R}^{N+1}$, collecting the configuration $\mathbf{u} \in \mathbb{R}^N$ and the load multiplier $\lambda \in \mathbb{R}$, $\mathbf{s}[\mathbf{u}]$ is the *internal forces vector* and $\mathbf{p}$ the *reference load vector*. Eq.(2) represents a system of N-equations and $N+1$ unknowns and defines the *equilibrium path* as a curve in $\mathbb{R}^{N+1}$ from a known initial configuration $\mathbf{u}_0$, corresponding to $\lambda = 0$. We also define the tangent stiffness matrix as

$$\delta\mathbf{u}_2^T \mathbf{K}[\mathbf{u}]\delta\mathbf{u}_1 = \Phi''[u]\delta u_1 \delta u_2 \;\;,\;\; \forall\, \delta\mathbf{u}_1, \delta\mathbf{u}_2 \tag{3}$$

where δu_i are generic variations of the configuration field u and $\delta\mathbf{u}_i$ the corresponding FE vectors.

where δu_i are generic variations of the configuration field u and $\delta\mathbf{u}_i$ the corresponding FE vectors.

2.2. Path–following analysis

The Riks approach [22] completes the equilibrium equations (2) with the additional constraint $g[\mathbf{u}, \lambda] - \xi = 0$, which defines a surface in $\mathbb{R}^{N+1}$. Assigning successive values to the control parameter $\xi = \xi_{(k)}$ the solution of the non-linear system

$$\mathbf{R}[\xi] \equiv \begin{bmatrix} \mathbf{r}[\mathbf{u}, \lambda] \\ g[\mathbf{u}, \lambda] - \xi \end{bmatrix} = \mathbf{0} \tag{4}$$

defines a sequence of points (steps) $\mathbf{z}_{(k)} \equiv \{\mathbf{u}_{(k)},\, \lambda_{(k)}\}$ belonging to the equilibrium path. Starting from a known equilibrium point $\mathbf{z}^0 \equiv \mathbf{z}_{(k)}$, the new one

$\mathbf{z}_{(k+1)}$ is evaluated correcting a first *extrapolation* $\mathbf{z}^1 = \{\mathbf{u}^1,\, \lambda^1\}$ by a sequence of estimates $\mathbf{z}^j$ (loops) by a Newton–Raphson iteration

$$\begin{cases} \tilde{\mathbf{J}}\dot{\mathbf{z}} = -\mathbf{R}^j \\ \mathbf{z}^{j+1} = \mathbf{z}^j + \dot{\mathbf{z}} \end{cases} \tag{5a}$$

where $\mathbf{R}^j \equiv \mathbf{R}[\mathbf{z}^j]$ and $\tilde{\mathbf{J}}$ is the Jacobian of the non-linear system (4) at $\mathbf{z}^j$ or its suitable estimate. The simplest choice for $g[\mathbf{u}, \lambda]$ is the linear constraint corresponding to the orthogonal hyperplane

$$\mathbf{n}_u^T(\mathbf{u} - \mathbf{u}^j) + n_\lambda\,(\lambda - \lambda^j) = \Delta\xi \quad \text{where} \quad \begin{cases} \mathbf{n}_u \equiv \mathbf{M}\,(\mathbf{u}^j - \mathbf{u}_{(k)}) \\ \mathbf{n}_\lambda \equiv \mu\,(\lambda^j - \lambda_{(k)}) \end{cases} \tag{5b}$$

$\mathbf{M}$ and μ being some suitable metric factors [16, 19], $\Delta\xi$ an assigned increment of ξ and

$$\tilde{\mathbf{J}} \approx \left[\frac{\partial \mathbf{R}[\mathbf{z}]}{\partial \mathbf{z}}\right]_{\mathbf{z}^j} = \begin{bmatrix} \tilde{\mathbf{K}} & -\hat{\mathbf{p}} \\ \mathbf{n}_u^T & n_\lambda \end{bmatrix} \tag{5c}$$

The load-controlled scheme is obtained assuming $g[\mathbf{u}, \lambda] = \lambda$ (see [16] for further details) while keeping $\tilde{\mathbf{K}} = \mathbf{K}[\mathbf{u}^1]$ we have the modified Newton-Raphson scheme. The solution of Eq.(5) is conveniently performed as follows

$$\begin{cases} \dot{\lambda} = \dfrac{\mathbf{n}_u^T \tilde{\mathbf{K}} \mathbf{r}^j}{n_\lambda + \mathbf{n}_u^T \tilde{\mathbf{K}} \mathbf{p}} \\ \tilde{\mathbf{K}}\dot{\mathbf{u}} = \dot{\lambda}\mathbf{p} - \mathbf{r}^j \end{cases} \tag{5d}$$

The convergence of the iterative process (5) has been widely discussed in [16, 21] and can be expressed in the condition

$$\mathbf{R}^{j+1} = \left(\mathbf{I} - \mathbf{J}_s \tilde{\mathbf{J}}^{-1}\right) \mathbf{R}^j \tag{5e}$$

where $\mathbf{I}$ is the identity matrix and $\mathbf{J}_s \equiv \int_0^1 \mathbf{J}[\mathbf{z}^j + t(\mathbf{z}^{j+1} - \mathbf{z}^j)]\; dt$ the secant Jacobian matrix. The convergence is as fast as

$$\mathbf{u}^T \mathbf{K}_s \mathbf{u} \approx \mathbf{u}^T \tilde{\mathbf{K}} \mathbf{u}, \quad \forall \mathbf{u} \tag{5f}$$

and the method converges in a single iteration when $\tilde{\mathbf{K}} = \mathbf{K}_s$ because of the linearity of Eq.(5b).

2.3. Displacement-based FE

In displacement-based FE formulations only the displacement field is interpolated in the domain and, thus,

$$\mathbf{u}[\boldsymbol{\xi}] = \mathbf{N}_d[\boldsymbol{\xi}]\mathbf{d}_e \tag{6}$$

where $\mathbf{d}_e$ are the element discrete DOFs, linked to the global ones $\mathbf{d}$ by the relation $\mathbf{d}_e = \mathbf{A}_e\mathbf{d}$ and $\boldsymbol{\xi}$ are the coordinates used to express the FE interpolation. The dependence on the coordinates will be omitted in the following in order to simplify the notation. The strain energy can be expressed as a sum of element contributions $\Phi[u] \equiv \sum_e \Phi_e[u]$, where, letting V_e the finite element domain and $\mathbf{C}$ the constitutive matrix,

$$\Phi_e[u] \equiv \int_{V_e} \left(\frac{1}{2}\boldsymbol{\varepsilon}^T\mathbf{C}\boldsymbol{\varepsilon}\right) dV_e \tag{7}$$

and the strains or generalized strains $\boldsymbol{\varepsilon} = \mathcal{D}[\mathbf{u}]\mathbf{u}$, introducing the interpolation in (32), assume the general form

$$\boldsymbol{\varepsilon} = \mathbf{B}[\mathbf{d}_e]\mathbf{d}_e, \tag{8}$$

with the differential operator $\mathcal{D}$ and its discrete counterpart $\mathbf{B}$, in general, nonlinear in $\mathbf{u}$ and $\mathbf{d}_e$ respectively. The first variation of the strain measure can be written as

$$\delta\boldsymbol{\varepsilon} = \mathbf{Q}[\mathbf{d}_e]\delta\mathbf{d}_e$$

and, then, the first variation of the strain energy is

$$\Phi_e[u]'\delta u \equiv \int_{V_e} \left(\delta\boldsymbol{\varepsilon}^T\mathbf{C}\boldsymbol{\varepsilon}\right) dV_e = \int_{V_e} \left(\delta\mathbf{d}_e^T\mathbf{Q}[\mathbf{d}_e]^T\mathbf{C}\mathbf{B}[\mathbf{d}_e]\mathbf{d}_e\right) dV_e = \delta\mathbf{d}_e^T\mathbf{s}_e[\mathbf{d}_e] \tag{9}$$

where $\mathbf{s}_e[\mathbf{d}_e]$ is the element internal forces vector. The second variation of the strain measure is

$$\delta\dot{\boldsymbol{\varepsilon}} = \boldsymbol{\mathcal{Q}}[\mathbf{d}_e, \dot{\mathbf{d}}_e]\delta\mathbf{d}_e = \boldsymbol{\mathcal{Q}}[\mathbf{d}_e, \delta\mathbf{d}_e]\dot{\mathbf{d}}_e$$

and its kth component is written as

$$\delta\dot{\varepsilon}_k = \dot{\mathbf{d}}_e^T\boldsymbol{\Psi}_k[\mathbf{d}_e]\delta\mathbf{d}_e$$

As $\boldsymbol{\sigma} = \mathbf{C}\boldsymbol{\varepsilon}$, the following expression holds

$$\boldsymbol{\sigma}^T \delta\dot{\boldsymbol{\varepsilon}} \equiv \sum_k \sigma_k \delta\dot{\varepsilon}_k = \dot{\mathbf{d}}_e^T \boldsymbol{\mathcal{G}}[\boldsymbol{\sigma}, \mathbf{d}_e]\delta\mathbf{d}_e$$

with

$$\boldsymbol{\mathcal{G}}[\boldsymbol{\sigma}[\mathbf{d}_e], \mathbf{d}_e] = \sum_k \sigma_k[\mathbf{d}_e]\boldsymbol{\Psi}_k[\mathbf{d}_e]\mathbf{d}_e \tag{10}$$

The second variation of the strain energy is

$$\Phi_e''[u]\delta u\dot{u} \equiv \int_{V_e} \left(\delta\boldsymbol{\varepsilon}^T \mathbf{C}\dot{\boldsymbol{\varepsilon}} + \delta\dot{\boldsymbol{\varepsilon}}^T \mathbf{C}\boldsymbol{\varepsilon}\right) dV_e = \delta\mathbf{d}_e^T \mathbf{K}_e[\mathbf{d}_e]\dot{\mathbf{d}}_e \tag{11}$$

with the element tangent stiffness matrix defined as

$$\mathbf{K}_e[\mathbf{d}_e] \equiv \int_{V_e} \left(\mathbf{Q}[\mathbf{d}_e]^T \mathbf{C}\mathbf{Q}[\mathbf{d}_e] + \boldsymbol{\mathcal{G}}[\boldsymbol{\sigma}[\mathbf{d}_e], \mathbf{d}_e]\right) dV_e \tag{12}$$

2.3.1. Numerical integration

The evaluation of the internal force vector and the tangent stiffness matrix, starting from the strain energy expression, requires integrations over the FE domain. The standard technique, usually employed to perform the integrations, is the Gauss quadrature, which allows the evaluation of the strain energy as

$$\Phi_e[\mathbf{d}_e] \equiv \sum_g^n \left(\frac{1}{2}\boldsymbol{\varepsilon}_g[\mathbf{d}_e]^T \mathbf{C}_g \boldsymbol{\varepsilon}_g[\mathbf{d}_e]\right) w_g \tag{13}$$

where subscript g denotes quantities evaluated in the integration point $\boldsymbol{\xi}_g$ and w_g is the corresponding weight. If the coordinates $\boldsymbol{\xi}$ in Eq.(32) are not the physical ones, w_g includes the determinant of the Jacobian matrix of the coordinate transformation, evaluated in the Gauss point. The internal forces vector becomes

$$\mathbf{s}_e[\mathbf{d}_e] = \sum_g^n \left(\boldsymbol{\mathcal{B}}_g[\mathbf{d}_e]^T \mathbf{C}_g \boldsymbol{\varepsilon}_g[\mathbf{d}_e]\right) w_g \tag{14}$$

while the tangent stiffness matrix is

$$\mathbf{K}_e[\boldsymbol{\sigma}_g[\mathbf{d}_e], \mathbf{d}_e] = \sum_g^n \left(\boldsymbol{\mathcal{B}}_g[\mathbf{d}_e]^T \mathbf{C}_g \boldsymbol{\mathcal{B}}_g[\mathbf{d}_e] + \boldsymbol{\mathcal{G}}_g[\boldsymbol{\sigma}_g[\mathbf{d}_e], \mathbf{d}_e]\right) w_g \tag{15}$$

where $\mathbf{K}_e[\mathbf{d}_e]$ is written as $\mathbf{K}_e[\boldsymbol{\sigma}_g[\mathbf{d}_e], \mathbf{d}_e]$ as a reminder of the way it is computed.

2.3.2. Remarks

It is important to note that $\mathbf{K}_e$ in Eq.(12) contains the term $\boldsymbol{\mathcal{G}}[\boldsymbol{\sigma}[\mathbf{d}_e], \mathbf{d}_e]$, that depends on the stress evaluated using the current displacements $\mathbf{d}_e$. The true stresses, in large displacement and small strain problems, slowly change along the equilibrium path. Unfortunately, during an iterative process, $\mathbf{d}_e$ is just a current estimate and then, $\boldsymbol{\sigma}[\mathbf{d}_e] = \mathbf{C}\boldsymbol{\varepsilon}[\mathbf{d}_e]$, that is a non-linear function of $\mathbf{d}_e$, can be very different from the stresses of the near equilibrium points. This "bad" stress estimate gets worse when the structure presents directions with very different stiffness ratios and undergoes finite rotations, because $\boldsymbol{\varepsilon}[\mathbf{d}_e]$, during the iterations, can have non realistic components even in the stiffest direction. This phenomenon leads to a slow convergence and an easy loss in convergence of the Newton method, because $\mathbf{K}_j$ can easily be far from the secant matrix in the convergence condition (5e). Conversely, mixed FE formulations are not affected by this phenomenon because the stresses are directly extrapolated and corrected. This difference in the iterative scheme is the reason why mixed FEs allow a faster convergence of the Newton method in path-following analyses and can withstand large step sizes (load increments). We refer readers to [21] for further details on this topic.

3. The new iterative scheme for displacement-based FEs based on mixed integration points

The performances of the Newton iterative method in geometrically non-linear problems discretized via displacement-based FEs are highly penalized by the constitutive constraint. On the contrary, the iterative scheme for mixed (stress-displacement) FE models is much faster and more robust.

The question we pose is the following: is it possible to exploit the advantages of the mixed iterative scheme for displacement-based FE models without changing the FE interpolation? In this section we give an effective answer, proposing a Newton method based on the relaxation of constitutive equations at the level of the integration points during the iterative process. The approach, called MIP

Newton (Mixed Integration Point), allows a significant improvement in the performances of the method, without affecting the discrete approximation of the FE and without upsetting the existing FE codes. In fact the proposed strategy consists of a few changes to the standard iterative method, which are simple implementation details, but the benefits in geometrically non-linear analysis are impressive, as will be shown in the numerical tests.

3.1. The MIP full Newton

The fundamental idea of the MIP Newton iterative scheme is to relax the constitutive equations at the level of each integration point. This is made by writing the total energy in a pseudo mixed form on the element

$$\Pi_e[\mathbf{u}_e] \equiv \Phi_e[\mathbf{u}_e] - \mathbf{d}_e^T \mathbf{p}_e \quad \text{with} \quad \mathbf{u}_e = \begin{bmatrix} \boldsymbol{\sigma}_1 \\ \vdots \\ \boldsymbol{\sigma}_n \\ \mathbf{d}_e \end{bmatrix} \tag{16}$$

where $\mathbf{p}_e$ is the element counterpart of the load vector $\mathbf{p}$ and the "mixed" strain energy $\Phi_e[\mathbf{u}_e]$ is obtained by rewriting Eq. (13) in a pseudo Helling-Reissner form as

$$\Phi_e[\mathbf{u}_e] \equiv \sum_{g=1}^{n} \left(\boldsymbol{\sigma}_g^T \boldsymbol{\varepsilon}_g[\mathbf{d}_e] - \frac{1}{2} \boldsymbol{\sigma}_g^T \mathbf{C}_g^{-1} \boldsymbol{\sigma}_g \right) w_g \tag{17}$$

in which the stresses at each integration point $\boldsymbol{\sigma}_g$ are now independent variables. The first variation of (17) is

$$\Phi'_e \delta u = \sum_{g=1}^{n} \begin{bmatrix} \delta\boldsymbol{\sigma}_g \\ \delta\mathbf{d}_e \end{bmatrix}^T \begin{bmatrix} \mathbf{s}_{g\sigma} \\ \mathbf{s}_{gd} \end{bmatrix} w_g \tag{18}$$

with

$$\begin{cases} \mathbf{s}_{g\sigma} \equiv \boldsymbol{\varepsilon}_g[\mathbf{d}_e] - \mathbf{C}^{-1}\boldsymbol{\sigma}_g \\ \mathbf{s}_{gd} \equiv \mathbf{Q}_g[\mathbf{d}_e]^T \boldsymbol{\sigma}_g \end{cases} \tag{19}$$

We have to note that

- the stationary of (16) with respect to $\boldsymbol{\sigma}_g$ leads to the constitutive equations $\boldsymbol{\sigma}_g = \mathbf{C}_g \boldsymbol{\varepsilon}_g[\mathbf{d}_e]$ and, thus, the FE remains based on a displacement

formulation because the stresses satisfy the constitutive law along the equilibrium path exactly.

- the stresses at the integration points are primal variables and, thus, they are not forced to satisfy the constitutive law during the iterations but, the constitutive equations are solved together with the equilibrium equations and are satisfied only when convergence is obtained.

The second variation of (16) is

$$\Phi''_e \delta u \dot{u} = \sum_{g=1}^{n} \begin{bmatrix} \delta\boldsymbol{\sigma}_g \\ \delta\mathbf{d}_e \end{bmatrix}^T \begin{bmatrix} -\mathbf{C}_g^{-1} & \boldsymbol{\mathcal{B}}_g \\ \boldsymbol{\mathcal{B}}_g^T & \boldsymbol{\mathcal{G}}_g \end{bmatrix} \begin{bmatrix} \dot{\boldsymbol{\sigma}}_g \\ \dot{\mathbf{d}}_e \end{bmatrix} w_g \tag{20}$$

where $\boldsymbol{\mathcal{G}}_g \equiv \boldsymbol{\mathcal{G}}_e[\boldsymbol{\sigma}_g, \mathbf{d}_e]$ is the matrix $\boldsymbol{\mathcal{G}}_e$ evaluated in the integration point g, that is now a function of the displacement DOFs and of the independent stresses $\boldsymbol{\sigma}_g$. The linear system in Eq.(5d), at the element level, becomes

$$\begin{bmatrix} -\mathbf{C}_1^{-1} w_1 & & & \boldsymbol{\mathcal{B}}_1 w_1 \\ & \ddots & & \vdots \\ & & -\mathbf{C}_n^{-1} w_n & \boldsymbol{\mathcal{B}}_n w_n \\ \boldsymbol{\mathcal{B}}_1^T w_1 & \dots & \boldsymbol{\mathcal{B}}_n^T w_n & \sum_g^n \boldsymbol{\mathcal{G}}_g w_g \end{bmatrix}^j \begin{bmatrix} \dot{\boldsymbol{\sigma}}_1 \\ \vdots \\ \dot{\boldsymbol{\sigma}}_n \\ \dot{\mathbf{d}}_e \end{bmatrix} = (\lambda^j + \dot{\lambda}) \begin{bmatrix} \mathbf{0} \\ \vdots \\ \mathbf{0} \\ \mathbf{p}_e \end{bmatrix} - \begin{bmatrix} \mathbf{s}_{1\sigma} w_1 \\ \vdots \\ \mathbf{s}_{n\sigma} w_n \\ \sum_g^n \left(\boldsymbol{\mathcal{B}}_g^T \boldsymbol{\sigma}_g w_g \right) \end{bmatrix}^j \tag{21}$$

where the superscript on matrices denotes that they are evaluated during the iterative process in the current estimate $\mathbf{u}_e^j$.

By performing a static condensation of the stresses $\dot{\boldsymbol{\sigma}}_g$, locally defined at the level of the integration point, we obtain

$$\dot{\boldsymbol{\sigma}}_g = \mathbf{C}_g \boldsymbol{\mathcal{B}}_g^j \dot{\mathbf{d}}_e + \mathbf{C}_g \mathbf{s}_{g\sigma}^j = \mathbf{C}_g \boldsymbol{\mathcal{B}}_g^j \dot{\mathbf{d}}_e + \mathbf{C}_g \boldsymbol{\varepsilon}_g^j - \boldsymbol{\sigma}_g^j \tag{22}$$

and letting $\mathbf{r}_{ce}[\mathbf{d}_e^j] = \mathbf{s}_{ce}[\mathbf{d}_e^j] - \lambda^j \mathbf{p}_e$

$$\mathbf{K}_e[\mathbf{u}_e^j] \dot{\mathbf{d}}_e = -\mathbf{r}_{ce}[\mathbf{d}_e^j] + \dot{\lambda} \mathbf{p}_e \tag{23}$$

with

$$\mathbf{K}_e[\boldsymbol{\sigma}_g^j, \mathbf{d}_e^j] = \sum_{g=1}^{n} \left(\boldsymbol{\mathcal{B}}_g[\mathbf{d}_e^j]^T \mathbf{C}_g \boldsymbol{\mathcal{B}}_g[\mathbf{d}_e^j] + \boldsymbol{\mathcal{G}}_g[\boldsymbol{\sigma}_g^j, \mathbf{d}_e^j] \right) w_g \tag{24}$$

the condensed tangent stiffness matrix, that has the same form as the classical displacement based one (15). However, this time it also depends on the independent stresses at the integration points, which are now directly extrapolated and corrected during the iterations.

Conversely, we can note that the condensed internal forces $\mathbf{s}_{ce}[\mathbf{d}_e^j]$

$$\mathbf{s}_{ce}[\mathbf{d}_e^j] = \sum_g^n \left(\boldsymbol{\mathcal{B}}_g^{j\,T} \mathbf{C}_g \boldsymbol{\varepsilon}_g^j \right) w_g$$

coincides exactly with the internal forces of the displacement-based formulation in Eq. (14). This iterative scheme is then very close to the standard Newton one for displacement-based FE models as it is highlighted in Tab. 1. The main difference consists of the different value of the stresses at the integration points used for the evaluation of the tangent stiffness matrix. In the Newton method the stresses $\boldsymbol{\sigma}_g$ are functions of the displacements and are forced to satisfy the constitutive law at each iteration. Conversely, in the MIP Newton $\boldsymbol{\sigma}_g$ are primal variables and so, are directly extrapolated and corrected and only at convergence satisfy the constitutive law. Clearly, the equilibrium path recovered is the same as the standard displacement approach, but the proposed method requires a much lower number of iterations, under equal convergence criteria, and can withstand larger step sizes (load increments). The improved performances are mainly due to the "better" iteration matrix that is possible when the stresses, which slowly change along the equilibrium path and during the iterations, are chosen as primal variables of the iterative scheme. Furthermore, it is possible to note, looking at Tab. 1, that the computational cost of a MIP iteration is practically the same as a standard one.

3.2. The MIP modified Newton

The modified Newton method evaluates and decomposes the iteration matrix in the first extrapolation (predictor) of each step. If the matrix is a good approximation of the secant one the method can converge in a reasonable number of iterations. Unfortunately, in geometrically non-linear analysis, displacement-based FEs usually prevent the use of the modified scheme. In fact, already

	Newton	**MIP Newton**
Predictor	$\mathbf{d}^1 = \mathbf{d}_{(k)} + \Delta\mathbf{d}$ $\lambda^1 = \lambda_{(k)} + \Delta\lambda$ $\boldsymbol{\sigma}_g[\mathbf{d}^1] = \mathbf{C}_g\boldsymbol{\varepsilon}_g[\mathbf{d}^1]$	$\mathbf{d}^1 = \mathbf{d}_{(k)} + \Delta\mathbf{d}$ $\lambda^1 = \lambda_{(k)} + \Delta\lambda$ $\boldsymbol{\sigma}_g^1 = \boldsymbol{\sigma}_{g(k)} + \Delta\boldsymbol{\sigma}_g$
Iteration matrix	$\mathbf{K}[\boldsymbol{\sigma}_g[\mathbf{d}^j], \mathbf{d}^j]$	$\mathbf{K}[\boldsymbol{\sigma}_g^j, \mathbf{d}^j]$
Residual vector	$\mathbf{s}[\mathbf{d}^j] - \lambda^j\mathbf{p}$	$\mathbf{s}[\mathbf{d}^j] - \lambda^j\mathbf{p}$
New estimate	$\mathbf{d}^{j+1} = \mathbf{d}^j + \dot{\mathbf{d}}$ $\lambda^{j+1} = \lambda^j + \dot{\lambda}$ $\boldsymbol{\sigma}_g^{j+1} = \mathbf{C}_g\boldsymbol{\varepsilon}_g[\mathbf{d}^{j+1}]$	$\mathbf{d}^{j+1} = \mathbf{d}^j + \dot{\mathbf{d}}$ $\lambda^{j+1} = \lambda^j + \dot{\lambda}$ $\boldsymbol{\sigma}_g^{j+1} = \boldsymbol{\sigma}_g^{j+1} + \dot{\boldsymbol{\sigma}}$

Table 1: Schematic description of the principal point of the algorithms: the differences between the standard Newton and the MIP Newton are marked in red.

failure easily occurs for the full Newton and is assured for the modified method unless a very small step size and a very large number of iterations are used. This is not the case with the previously proposed MIP Newton scheme. In fact, the stiffness matrix, evaluated using the direct extrapolation of the stresses from the previous step, is already a good estimation of the secant matrix and, furthermore, the MIP tangent matrix slightly changes during the iterative process. The matrix so evaluated in the first prediction is then suitable for use in all the iterations over the step, as required in the modified version of the method (MIP modified Newton). Clearly, the number of iterations required by MIP modified Newton is larger than that required by the MIP full Newton, but the direct extrapolation of the stress assures robustness and efficiency. The few extra-iterations are compensated by the need to calculate and decompose the iteration matrix just once in each step.

The linear system in Eq.(5d) can be written as

$$\begin{bmatrix} -\mathbf{C}_1^{-1} w_1 & & & \boldsymbol{\mathcal{B}}_1 w_1 \\ & \ddots & & \vdots \\ & & -\mathbf{C}_n^{-1} w_n & \boldsymbol{\mathcal{B}}_n w_n \\ \boldsymbol{\mathcal{B}}_1^T w_1 & \dots & \boldsymbol{\mathcal{B}}_n^T w_n & \sum_g^n \boldsymbol{\mathcal{G}}_g w_g \end{bmatrix}^1 \begin{bmatrix} \dot{\boldsymbol{\sigma}}_1 \\ \vdots \\ \dot{\boldsymbol{\sigma}}_n \\ \dot{\mathbf{d}}_e \end{bmatrix} = (\lambda^j + \dot{\lambda}) \begin{bmatrix} \mathbf{0} \\ \vdots \\ \mathbf{0} \\ \mathbf{p}_e \end{bmatrix} - \begin{bmatrix} \mathbf{s}_{1\sigma} w_1 \\ \vdots \\ \mathbf{s}_{n\sigma} w_n \\ \sum_g^n \left(\boldsymbol{\mathcal{B}}_g^T \boldsymbol{\sigma}_g w_g \right) \end{bmatrix}^j \tag{25}$$

where the superscript 1 denotes quantities evaluated in the first prediction of the new equilibrium point. By performing a static condensation of the stresses $\boldsymbol{\sigma}_g$, locally defined at the level of each integration point, we obtain

$$\dot{\boldsymbol{\sigma}}_g = \mathbf{C}_g \boldsymbol{\mathcal{B}}_g[\mathbf{d}_e^1] \dot{\mathbf{d}}_e + \mathbf{C}_g \mathbf{s}_{g\sigma}^j = \mathbf{C}_g \boldsymbol{\mathcal{B}}_g[\mathbf{d}_e^1] \dot{\mathbf{d}}_e + \mathbf{C}_g \boldsymbol{\varepsilon}_g^j - \boldsymbol{\sigma}_g^j \tag{26}$$

and letting $\mathbf{r}_{ce}[\mathbf{d}_e^j] = \mathbf{s}_{ce}[\mathbf{d}_e^j] - \lambda^j \mathbf{p}_e$

$$\mathbf{K}_e[\mathbf{u}_e^1] \dot{\mathbf{d}}_e = -\mathbf{r}_{ce}[\mathbf{d}_e^j] + \dot{\lambda} \mathbf{p}_e \tag{27}$$

where

$$\mathbf{K}[\mathbf{u}_e^j] = \sum_{g=1}^{n} \left(\boldsymbol{\mathcal{B}}_g[\mathbf{d}_e^1]^T \mathbf{C}_g \boldsymbol{\mathcal{B}}_g[\mathbf{d}_e^1] + \boldsymbol{\mathcal{G}}_g[\boldsymbol{\sigma}_g^1, \mathbf{d}_e^1] \right) w_g \tag{28}$$

is the iteration matrix, constant during the iterations of the single step. In the MIP modified Newton scheme we have to note that, with respect to the MIP full method, the condensed internal force vector

$$\mathbf{s}_{ce}[\mathbf{d}_e^j] = \sum_{g}^{n} \left(\boldsymbol{\mathcal{B}}_g[\mathbf{d}_e^j]^T \boldsymbol{\sigma}_g^j + \boldsymbol{\mathcal{B}}_g[\mathbf{d}_e^1]^T (\mathbf{C}_g \boldsymbol{\varepsilon}_g^j - \boldsymbol{\sigma}_g^j) \right) w_g \neq \mathbf{s}_e[\mathbf{d}_e^j]$$

does not coincide with that of the displacement-based scheme, because of the use of a constant iteration matrix. However, this is just a further implementation detail with a very low extra-cost cost, compensated by the constant iteration matrix.

Note that, even in this case, the stresses, at convergence but not during the iterative process, satisfy the constitutive law exactly and so the method provides the same equilibrium path as the standard displacement-based approach. However, note that the estimated iteration matrix in the modified MIP-Newton is so "good" that usually the number of iterations required is even less than that required by the standard full Newton for displacement-based FE models.

4. Implementation details

The impressive better performances of the proposed iterative strategy with respect to the standard Newton method hold for any structural model, displacement–based finite element and implementation choice of the Newton method and of the arc-length constraint. However, in this section, some details about all these aspects are provided, in order to make the numerical tests presented in the next section reproducible. In particular the structural models considered are chosen to be as simple and general as possible: i) 2D frames, based on the Antman geometrically exact strain measure; ii) 3D shells, based on a solid-shell FE model and the Green-Lagrange strain measure. A Total Lagrangian formulation is chosen for both the models, even if other formulations can be easily employed.

4.1. Implementation details of the Newton scheme

- Predictor

  Starting from a known equilibrium point $\mathbf{z}_k$ the first predictor $\mathbf{z}_k^1$ of the new equilibrium point $\mathbf{z}_{k+1}$ is evaluated as

  $$\mathbf{z}_1 = \mathbf{z}_k + \alpha(\mathbf{z}_k - \mathbf{z}_{k-1})$$

  where α defines the step size. For the first equilibrium point it is particularized as

  $$\mathbf{z}_1 = \Delta\lambda_0 \begin{bmatrix} 1 \\ \hat{\mathbf{u}} \end{bmatrix}$$

  being $\hat{\mathbf{u}}$ the linear elastic solution for the reference load $\mathbf{p}$.

- Arc-length parameters

  The arc-length constraint in Eq.(5b) is defined by the metric factors $\mathbf{M}$ and μ. The metric matrix $\mathbf{M}$ is assumed to be a diagonal matrix with $M_{ii} = 1$ if the ith variable is a displacement, $M_{ii} = \ell^2$ if the ith variable is a rotation, ℓ being a characteristic length of the structures. The factor μ is selected as

  $$\mu = \mu_0^2 \hat{\mathbf{d}}^T \mathbf{M} \hat{\mathbf{d}}$$

where the factor μ_0, chosen to be equal to 10^{-2}, takes into account that for stability problems the initial tangent can be much larger than the average one.

- The adaptive step size

  The factor α which defines the step size is evaluated in an adaptive way in terms of the iterations required in the last step N_k and the desired number of iterations per step N_d, chosen as equal to 4, as

  $$\alpha = 1 - \frac{0.5(N_k - N_d)}{N_k + N_d}$$

  The values of α are constrained by the condition $\alpha \in [0.5, 2]$.

- Convergence criteria

  Convergence is accepted if

  $$(\dot{\mathbf{d}}^j)^T \mathbf{M} \dot{\mathbf{d}}^j < \text{Toll}^2 (\Delta\lambda_0^2 \hat{\mathbf{d}}^T \mathbf{M} \hat{\mathbf{d}})$$

  that is if the norm of the correction to the displacement solution is smaller than a desired tolerance Toll $= 10^{-4}$ compared to the initial solution increment. If the convergence condition is not satisfied after 20 iterations or if the error fails to decrease after two consecutive iterations, the iterations are abandoned and α is halved. After 5 consecutive divergent attempts, the process is declared failed.

- The load-controlled analysis

  A load-controlled analysis can be performed by redefining the arc-length constraint as

  $$\lambda = \lambda_{k+1}$$

  and setting $\alpha = 1$.

4.2. The 2D beam element

The 2D beam model is based on the objective Reissner-Antman strain measure

$$\boldsymbol{\varepsilon} = \begin{bmatrix} \epsilon \\ \gamma \\ \chi \end{bmatrix} \quad \text{with} \quad \begin{cases} \epsilon = (1 + u_{,s}) \cos\varphi + w_{,s} \sin\varphi - 1 \\ \gamma = -(1 + u_{,s}) \sin\varphi + w_{,s} \cos\varphi \\ \chi = \varphi_{,s} \end{cases} \tag{29}$$

where u, w, φ are, respectively, the axial displacement, the transversal displacement and the rotation, functions of the abscissa along the beam axis s. The constitutive matrix is

$$\mathbf{C} = \begin{bmatrix} EA & 0 & 0 \\ 0 & GAr & 0 \\ 0 & 0 & EJ \end{bmatrix} \tag{30}$$

where E is the Young modulus, G is the shear modulus, A is the cross-section area, r is the shear correction factor and J is the cross-section moment of inertia. The finite element is assumed to be straight and the FE interpolation is very simple and consists of a 3 node quadratic Lagrangian interpolation for u, w, φ. The nodes are located at the ends and at the midspan of the element.

The interpolation of u, w, φ is introduced in Eq.(29) so obtaining the operator $\mathbf{B}$ in Eq.(8).

Two Gauss integration points are used to evaluate the internal force vector and the stiffness matrix.

4.3. The solid-shell element

For the shell structures a solid-shell element is used. However, the MIP method can also easily be used for standard shell elements [23, 24].
The solid-shell element is based the interpolation described in [14]. It is presented here in the case of a Green-Lagrange strain measure and in a Total Lagrangian description. Denoting with $\boldsymbol{\xi} = \{\xi, \eta, \zeta\}$ the convective coordinates used to express the FE interpolation, the current configuration is described by the reference position vector $\mathbf{X}[\boldsymbol{\xi}] \equiv \{X[\boldsymbol{\xi}], Y[\boldsymbol{\xi}], Z[\boldsymbol{\xi}]\}$ and by the displacement

field $\mathbf{d}[\boldsymbol{\xi}]$. Adopting the convention of summing on repeated indexes, the covariant Green-Lagrange strain measure components are

$$\bar{E}_{ij} = \frac{1}{2}\left(\mathbf{X}_{,i}\cdot\mathbf{d}_{,j} + \mathbf{d}_{,i}\cdot\mathbf{X}_{,j} + \mathbf{d}_{,i}\cdot\mathbf{d}_{,j}\right) \quad \text{with} \quad i,j = \xi,\eta,\zeta \tag{31}$$

where a comma followed by k denotes the derivative with respect to k and $(\cdot)$ denotes the scalar product. The position vector of a point inside the element and its displacement are interpolated, using a trilinear 8 node hexahedron, as

$$\mathbf{X}[\boldsymbol{\xi}] = \mathbf{N}_d[\boldsymbol{\xi}]\mathbf{X}_e \quad , \quad \mathbf{d}[\boldsymbol{\xi}] = \mathbf{N}_d[\boldsymbol{\xi}]\mathbf{d}_e \tag{32}$$

where vectors $\mathbf{d}_e$ and $\mathbf{X}_e$ collect the element nodal displacements and coordinates and matrix $\mathbf{N}_d[\boldsymbol{\xi}]$ the trilinear interpolation functions. Adopting a Voigt notation the Green-Lagrange covariant strain components in Eq.(31) are collected in vector $\bar{\mathbf{E}} \equiv [\bar{E}_{\xi\xi}, \bar{E}_{\eta\eta}, 2\bar{E}_{\xi\eta}, \bar{E}_{\zeta\zeta}, 2\bar{E}_{\eta\zeta}, 2\bar{E}_{\xi\zeta}]^T$ that, exploiting Eq.(32), becomes

$$\bar{\mathbf{E}} = \left(\boldsymbol{\mathcal{L}}[\boldsymbol{\xi}] + \frac{1}{2}\boldsymbol{\mathcal{Q}}[\boldsymbol{\xi}, \mathbf{d}_e]\right)\mathbf{d}_e, \tag{33}$$

In order to circumvent shear and trapezoidal lockings, the natural transverse normal strain $\bar{E}_{\zeta\zeta}$ and the shear strains $\bar{E}_{\xi\zeta}, \bar{E}_{\eta\zeta}$ are redefined by the *assumed natural strain* (ANS) technique [25, 26, 27], assuming from now on that the Z-axis and the X-Y-plane are parallel to the ζ-axis and mid-surface of the shell respectively. To enhance the in-plane bending response of the element, the in-plane shear strain $\bar{E}_{\xi\eta}$ is substituted by its counterpart evaluated in $\xi = \eta = 0$, as a selective reduced integration (SRI). The covariant strains can be linearized with respect to ζ in the following form

$$\bar{\mathbf{E}} \approx \begin{bmatrix} \bar{\mathbf{e}}[\xi,\eta] + \zeta\ \bar{\boldsymbol{\chi}}[\xi,\eta] \\ \bar{E}_{\zeta\zeta}[\xi,\eta] \\ \bar{\boldsymbol{\gamma}}[\xi,\eta] \end{bmatrix} \tag{34}$$

where

$$\bar{\mathbf{e}}[\xi,\eta] \equiv \begin{bmatrix} \bar{E}_{\xi\xi} \\ \bar{E}_{\eta\eta} \\ 2\bar{E}_{\xi\eta} \end{bmatrix} \quad \bar{\boldsymbol{\chi}}[\xi,\eta] \equiv \begin{bmatrix} \bar{E}_{\xi\xi,\zeta} \\ \bar{E}_{\eta\eta,\zeta} \\ 2\bar{E}_{\xi\eta,\zeta} \end{bmatrix} \quad \bar{\boldsymbol{\gamma}}[\xi,\eta] \equiv \begin{bmatrix} 2\bar{E}_{\eta\zeta} \\ 2\bar{E}_{\xi\zeta} \end{bmatrix}$$

The generalized covariant strains can be collected in vector $\bar{\boldsymbol{\varepsilon}}$ as

$$\bar{\boldsymbol{\varepsilon}}[\xi,\eta] \equiv \begin{bmatrix} \bar{\mathbf{e}} \\ \bar{E}_{\zeta\zeta} \\ \bar{\boldsymbol{\chi}} \\ \bar{\boldsymbol{\gamma}} \end{bmatrix} = \left(\boldsymbol{\mathcal{L}}_\rho[\xi,\eta] + \frac{1}{2}\boldsymbol{\mathcal{Q}}_\rho[\xi,\eta,\mathbf{d}_e] \right) \mathbf{d}_e, \tag{35}$$

where matrix $\boldsymbol{\mathcal{L}}_\rho$ and $\boldsymbol{\mathcal{Q}}_\rho$ are automatically defined from Eq.(33) exploiting ASN, SRI and Eq.(34), so obtaining the operator $\mathbf{B}$ in Eq.(8).

Finally the generalized Cartesian strains are obtained from the natural ones as

$$\boldsymbol{\varepsilon} = \mathbf{T}\bar{\boldsymbol{\varepsilon}} \quad \text{with} \quad \mathbf{T}[\xi,\eta] = \begin{bmatrix} \mathbf{T}_p & 0 & 0 & 0 \\ 0 & T_z & 0 & 0 \\ 0 & 0 & \mathbf{T}_p & 0 \\ 0 & 0 & 0 & \mathbf{T}_t \end{bmatrix} \tag{36}$$

where, letting $\mathbf{J}$ the element Jacobian matrix, $T_z = 1/J_{33}^2$ and

$$\begin{aligned} \mathbf{T}_p &= \begin{bmatrix} J_{11}^2 & J_{12}^2 & 2J_{11}J_{12} \\ J_{21}^2 & J_{22}^2 & 2J_{21}J_{22} \\ J_{21}J_{11} & J_{22}J_{12} & J_{22}J_{11}+J_{21}J_{12} \end{bmatrix}^{-T} \\ \mathbf{T}_t &= \begin{bmatrix} J_{12}J_{33}+J_{13}J_{32} & J_{13}J_{31}+J_{11}J_{33} \\ J_{22}J_{33}+J_{23}J_{32} & J_{23}J_{31}+J_{21}J_{33} \end{bmatrix}^{-T} \end{aligned} \tag{37}$$

The generalized constitutive matrix $\mathbf{C}$ is evaluated starting from the constitutive law $\mathbf{S} = \mathbb{C}\mathbf{E}$, $\mathbf{S}$ being the second Piola-Kirchhoff stress tensor, performing an analytic pre-integration of $\mathbb{C}$ along the thickness direction and assuming a constant with Z stress S_{zz} instead of a constant thickness strain E_{zz}, in order to eliminate the thickness locking, following the approach proposed in [28].

A 2×2 grid of integration points on the middle plane of the shell is used to evaluate the internal force vector and the stiffness matrix.

The same format of the equation holds for other displacement based solid-shell elements [29].

5. Numerical tests

In this section some benchmarks concerning 2D framed structures and 3D shells are presented and discussed. The goal is to test and show the better performances of the proposed MIP approach with respect to the standard Newton method in terms of i) total number of iterations required to trace the equilibrium path or to obtain the deformed configuration for an assigned load, ii) the step size (or load increment) that the method can withstand without loss in convergence. We recall that for all the methods the convergence criteria and the analysis parameters are the same and are those reported in the previous section. Furthermore, we remember that all the methods, when converged, provide the same equilibrium path and deformed configurations.

In the comparisons of the different methods reported in the following, the term "Newton" denotes the standard full Newton method, "MIP Newton" denotes the full Newton based on the MIP approach and "MIP M. Newton" denotes the modified Newton based on the MIP approach.

5.1. 2D frame tests

The first tests are performed with a 2D beam model, based on the Antman strain measure and a quadratic Lagrangian FE interpolation for the displacements and the rotation. Two Gauss integration points are used. These simple numerical examples are presented because they are very easy to reproduce.

5.1.1. Clamped-Hinged arc

The first test is the clamped-hinged arc, already studied in many papers (see for example [16, 30]), for which the geometry, the loads and the material properties are reported in figure 1. A mesh of 18 finite elements has been used. The characteristic length used in the metric matrix to homogenize rotations and displacements is assumed as $\ell = R$.

The arc-length method with adaptive step size is adopted and the initial value of the load increment used is $\Delta\lambda_0 = 0.5$. The structure has been analyzed for different values of $k = AR^2/J$ to highlight the pathological dependence on

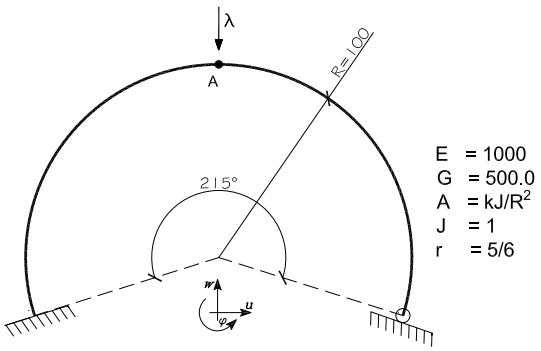

Figure 1: Clamped-hinged arc: geometry

	Newton		MIP Newton		MIP M. Newton	
k	steps	iters	steps	iters	steps	iters
10^5	124	507	41	138	61	240
10^6	193	833	41	138	61	240
10^7	401	1650	41	138	61	240

Table 2: Clamped-hinged arc: total number of steps and iterations for the evaluation of the equilibrium path.

this value of the robustness and performance of the path-following analysis. In Tab.2 the total number of steps and iterations required for the evaluation of the equilibrium path until a vertical displacement $w_A = -180$ is reported. We can observe that, even if the equilibrium path does not change for the considered values of k, the number of steps and total iterations required by the standard Newton drastically increases with k. Conversely, the performances of the MIP Newton, in both the full and the modified version are independent of k. In particular the MIP modified Newton, which requires only a matrix assemblage and factorization for each step, looks very convenient.

Finally in Fig.2 the equilibrium path and the evolution of the deformed configurations are presented.

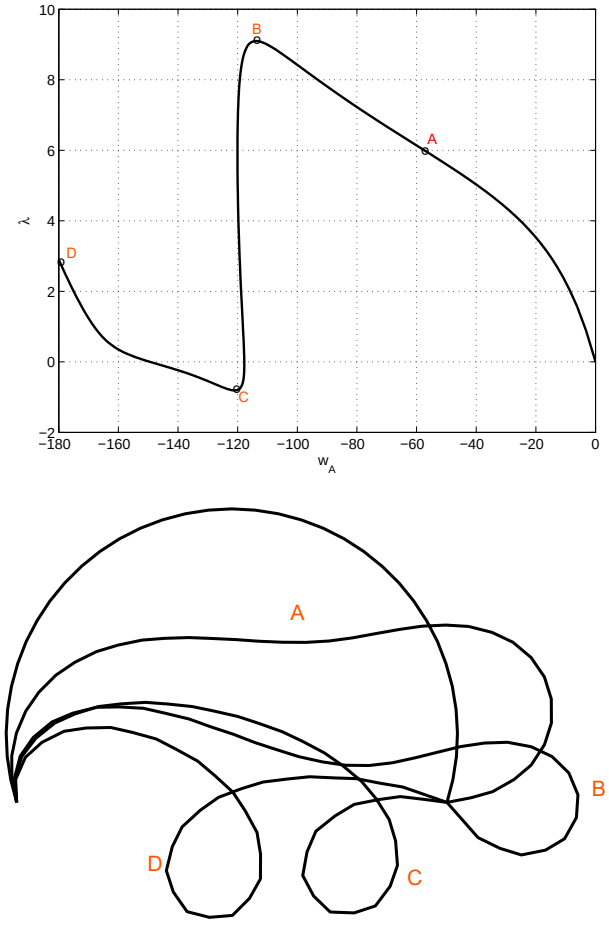

Figure 2: Clamped-hinged arc: equilibrium path and deformed configuration evolution

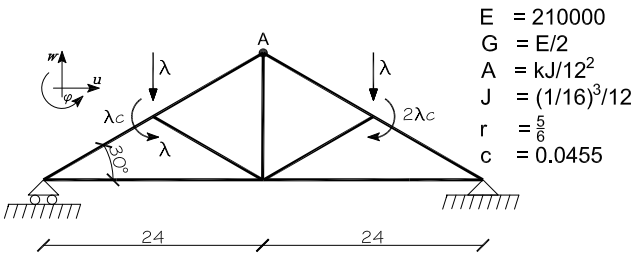

Figure 3: Rigidly jointed truss: geometry

5.1.2. Rigidly jointed truss

The second simple test consists of the rigidly jointed truss already studied in [16], for which the geometry, the loads and the material properties are reported in figure 3.

Six FEs for each beam have been used, while the initial load increment used in the arc-length strategy with adaptive step size is $\Delta\lambda_0 = 3.2$. The characteristic length used in the metric matrix to homogenize rotations and displacements is assumed as $\ell = H$, with H the truss height. Also in this case the structure has been analyzed for different values of $k = AH^2/J$ to highlight the effect of this value on the overall performance. In Tab. 3 the total number of steps and iterations required for the evaluation of the equilibrium path until a rotation $\varphi_A = -0.06$ is reported. Even in this case, the equilibrium path does not change for the considered values of k and we can observe the increasing number of steps and iterations required by the standard Newton. On the contrary, the MIP Newton, in both the full and the modified approach, is independent of k with the MIP modified Newton which, in this case, requires the same steps and loops as the MIP full one with a gain in computation.

Finally in Fig.4 the equilibrium path and the evolution of the deformed configurations are presented.

5.2. Shell structures

A series of popular benchmarks regarding shell structures in finite deformations are tested using the solid-shell element recalled in the previous section.

	Newton		MIP Newton		MIP M. Newton	
k	steps	iters	steps	iters	steps	iters
10^5	126	443	77	230	77	230
10^6	185	684	77	230	77	230
10^7	260	990	77	230	77	230

Table 3: Rigidly jointed truss: total number of steps and iterations for the evaluation of the equilibrium path.

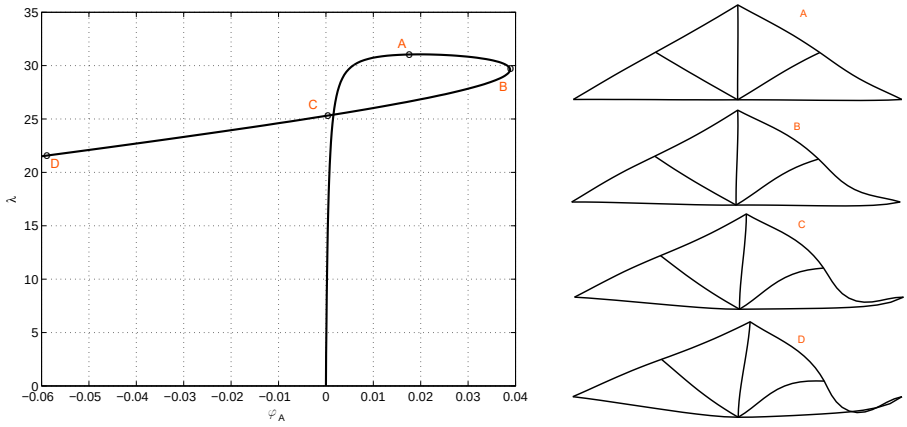

Figure 4: Rigidly jointed truss: equilibrium path and deformed configuration evolution

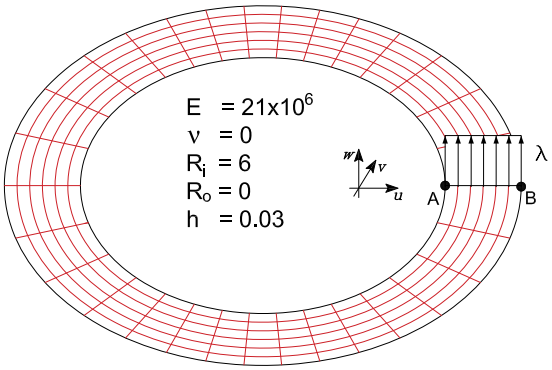

Figure 5: Slit annular plate: geometry

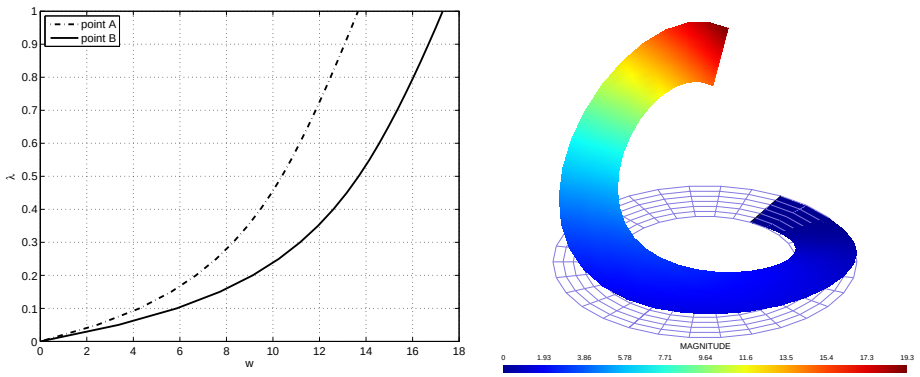

Figure 6: Slit annular plate: equilibrium path and deformed configuration at the last evaluated equilibrium point

5.3. Slit annular plate under line force

The first test is the slit annular plate described in Fig.5 and already analyzed by many authors [14, 31]. A mesh of 30×6 solid-shell FEs has been used.

In Fig.6 the equilibrium path and the evolution of the deformed configurations are presented.

To highlight the robustness of the proposed MIP Newton, the equilibrium path has been reconstructed using a load-controlled scheme. The maximum load value of 1 has been subdivided in $Nsteps$ equal load increments. The total number of iterations required to evaluate the equilibrium path are reported in

	Newton	MIP Newton	MIP M. Newton
$Nsteps$	iters	iters	iters
1	fails	9	fails
5	fails	20	fails
10	fails	32	44
20	175	54	58

Table 4: Slit annular plate: total number of iterations for the evaluation of the equilibrium path vs the number of load subdivisions.

Tab.4.

The standard Newton fails to converge with the first 3 load subdivisions, while for the finest one it converges but the number of iterations required is very high. Conversely, the MIP Newton is able to evaluate the equilibrium point corresponding to $\lambda = 1$ with just a single load increment and only 9 iterations. When the number of load steps $Nsteps$ increases, the number of iterations per step gets smaller, but the total number of iterations increases. However, even for the smallest step size the MIP Newton is more than three times more efficient than the standard Newton. Finally, the modified MIP Newton converges for reasonable values of the step size and with a number of iterations comparable with the full MIP Newton and much lower than that required by the standard full Newton.

5.4. Pinched cylinder with rigid diaphragms

Another interesting test regarding large deformations is the pinched cylinder depicted in Fig. 7 and also analyzed in [14, 31]. Exploiting the problem symmetries only an eighth of the cylinder is analyzed with a mesh of 40×40 solid-shell FEs.

In Fig.8 the equilibrium path and the evolution of the deformed configurations are presented.

In this case an arc-length technique with adaptive step size is employed with an initial load increment of $\Delta\lambda_0 = 300$. The total number of iterations

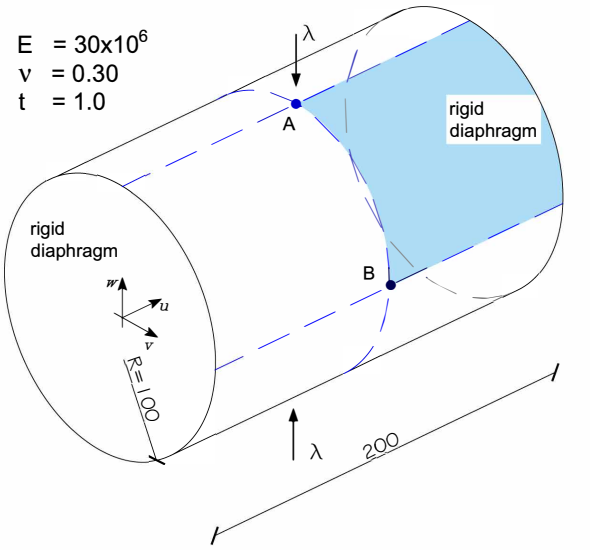

Figure 7: Pinched cylinder: geometry

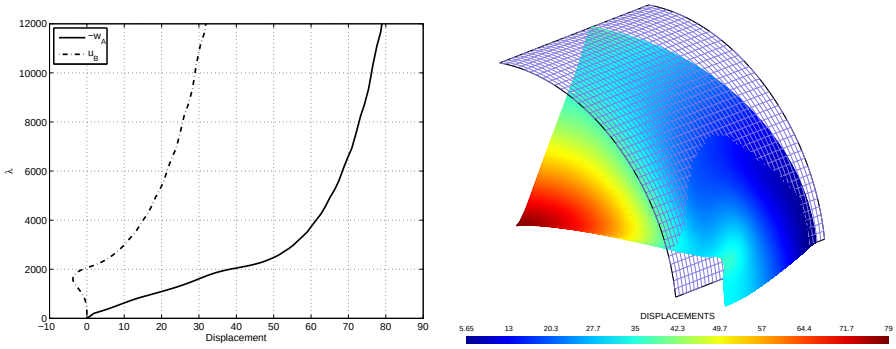

Figure 8: Pinched cylinder: equilibrium path and deformed configuration at the last evaluated equilibrium point

	steps	iters
Newton	135	543
MIP Newton	59	224
MIP M. Newton	86	338

Table 5: Pinched cylinder: total number of steps and iterations for the evaluation of the equilibrium path.

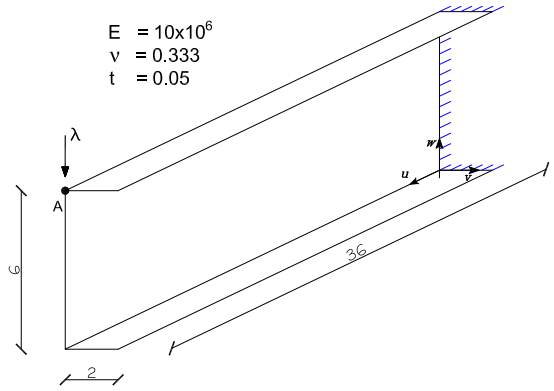

Figure 9: Thin walled cantilever beam: geometry

required to evaluate the equilibrium path are reported in Tab.5. Also in this case the great improvements of the MIP approach, in both full or modified Newton scheme, are evident.

5.5. Thin walled cantilever beam

Finally a test regarding a thin-walled cantilever beam with U cross section is considered. Geometry, loads and material properties are reported in Fig.9. The FE mesh consists of 2880 solid-shell FEs, obtained via 32 equal subdivisions on the cross section and 90 subdivisions along the beam axis. As shown in [32, 30, 33] the structure is characterized by complex buckling mode interaction phenomena.

An arc-length technique with adaptive step size is used and the initial load increment is $\Delta\lambda_0 = 3$. Fig.10 depicts the equilibrium path and the deformed

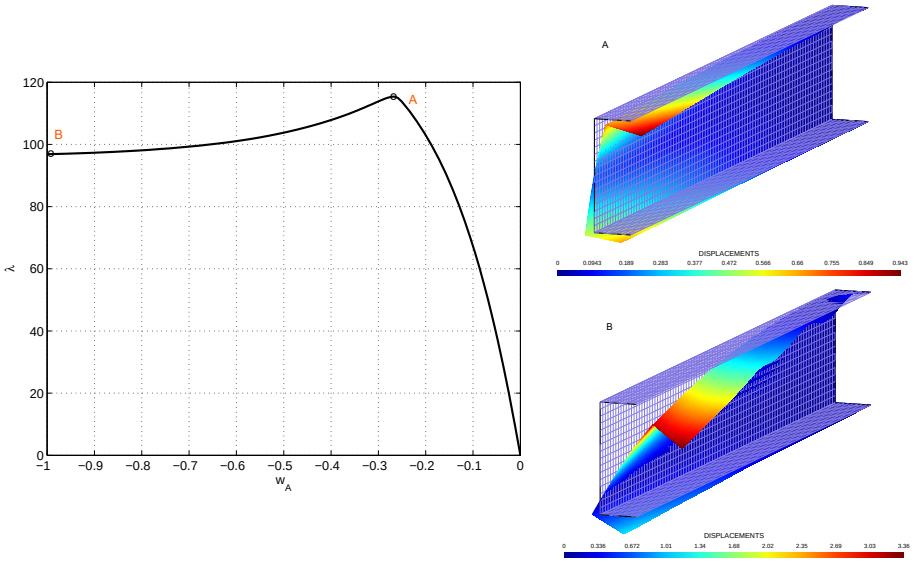

Figure 10: Cantilever beam: equilibrium path and deformed configuration at the last evaluated equilibrium point

	steps	iterations
Newton	82	301
MIP Newton	36	106
MIP M. Newton	55	175

Table 6: Thin-walled cantilever beam: total number of steps and iterations for the evaluation of the equilibrium path.

configuration at the limit and the final equilibrium point corresponding to a vertical displacement $w_A = 1$. The mode interaction is evident looking at the deformed shapes and produces the unstable post-critical behavior.

As for all the other tests, the MIP Newton, in both the full or the modified version, performs better with respect to the standard method as shown in Tab.6. In particular the full standard Newton requires a total number of iterations 3 times larger than the MIP full Newton and almost twice the MIP modified Newton.

6. Conclusion

In finite deformation problems discretized via displacement-based finite elements, the standard Newton method easily diverges unless a small step size is used. Even if it converges, often a large number of iterations are required. A new strategy, called MIP Newton, is proposed to improve the robustness and the efficiency of the iterative method in step-by-step geometrically non-linear analyses performed with displacement FE formulations. The approach proposed in this work is inspired by some previous studies regarding the advantages in the mixed (stress-displacement) formulation in geometrically non-linear problems. In particular, in [21] it was shown how the convergence of the Newton method in displacement formulation is penalized by the constitutive constraint, i.e. at each iteration the method is forced to satisfy the constitutive law.

The main idea of the MIP strategy, proposed here, consists in the relaxation of the constitutive law at the level of each integration point. In this way, the stresses at the integration points become primal variables in the iterative process and, thus they are directly extrapolated and corrected. The stresses are, then, no longer forced to satisfy the constitutive equations at each iteration, but the constitutive law is recovered exactly at convergence. In this way the discrete approximation of the finite element remains exactly the same, but the performances of the MIP Newton are impressive. As shown in many numerical tests, it allows us to solve finite deformation problems with a very low number of steps and total iterations, in step-by-step analysis, with respect to the standard Newton method. The advantages in terms of computational time are clear, considering that the cost of a MIP iteration is the same as a standard one. Moreover, the MIP Newton can withstand very large step sizes (load increments) without any loss in convergence, which are impossible using the standard Newton. The iteration matrix evaluated with the MIP strategy is so "good" that the modified version of the method, which computes and decomposes the iteration matrix at the first estimate of each equilibrium point, can also be conveniently adopted.

The inclusion of the MIP Newton in existing finite element codes is simple and only requires the modification of a few implementation details in the standard method. The proposed iterative strategy is so robust, efficient and simple that, in geometrically non-linear analysis, it is destined to replace the standard Newton method in any finite element code based on displacement formulations.

Future works will focus on the application of the MIP Newton in isogeometric analysis [34], where it is expected to have the same impact experienced in FE analysis. The proposal can be extended to other solution strategies such as the Koiter-Newton method [35, 36]. Efficient drape simulations [10] are also expected.

[1] R. Goncalves, M. Ritto-Correa, D. Camotim, A large displacement and finite rotation thin-walled beam formulation including cross-section deformation, Computer Methods in Applied Mechanics and Engineering 199 (23-24) (2010) 1627–1643. doi:10.1016/j.cma.2010.01.006.

[2] D. Dubina, V. Ungureanu, Instability mode interaction: From Van der Neut model to ECBL approach, Thin-Walled Structures 81 (2014) 39–49. doi:10.1016/j.tws.2013.10.014.

[3] A. Genoese, A. Genoese, A. Bilotta, G. Garcea, A geometrically exact beam model with non-uniform warping coherently derived from the Saint Venant rod, Engineering Structures 68 (2014) 33–46.

[4] E. Barbero, A. Madeo, G. Zagari, R. Zinno, G. Zucco, Koiter asymptotic analysis of folded laminated composite plates, Composites Part B: Engineering 61 (2014) 267–274, cited By 6. doi:10.1016/j.compositesb.2014.01.045.

[5] L. Friedrich, S. Loosen, K. Liang, M. Ruess, C. Bisagni, K.-U. Schräder, Stacking sequence influence on imperfection sensitivity of cylindrical composite shells under axial compression, Composite Structures 134 (2015) 750–761. doi:10.1016/j.compstruct.2015.08.132.

[6] S. R. Henrichsen, P. M. Weaver, E. Lindgaard, E. Lund, Post-buckling optimization of composite structures using koiter's method, International Journal for Numerical Methods in Engineering (2016) n/a–n/aNme.5239. doi:10.1002/nme.5239.
URL http://dx.doi.org/10.1002/nme.5239

[7] D. Magisano, L. Leonetti, G. Garcea, Koiter asymptotic analysis of multilayered composite structures, Composite Structures (2016) n/a–n/adoi:doi:http://dx.doi.org/10.1016/j.compstruct. 2016.07.046.

[8] L. A. Godoy, Thin Walled Structures with Structural Imperfections: Analysis and Behavior, Pergamon Press, Oxford, U.K., 1996.

[9] N. L. Rizzi, V. Varano, S. Gabriele, Initial postbuckling behavior of thin-walled frames under mode interaction, Thin-Walled Structures 68 (2013) 124 – 134. doi:http://dx.doi.org/10.1016/j.tws.2013.03.004.

[10] Q. Xie, K. Sze, Y. Zhou, Drape simulation using solid-shell elements and adaptive mesh subdivision, Finite Elements in Analysis and Design 106 (2015) 85–102. doi:10.1016/j.finel.2015.08.001.

[11] X. Liu, K. Sze, A corotational interpolatory model for fabric drape simulation, International Journal for Numerical Methods in Engineering 77 (6) (2009) 799–823. doi:10.1002/nme.2434.

[12] G. Garcea, G. Formica, R. Casciaro, A numerical analysis of infinitesimal mechanisms, International Journal for Numerical Methods in Engineering 62 (8) (2005) 979–1012. doi:10.1002/nme.1158.

[13] M. Duan, An efficient hybrid/mixed element for geometrically nonlinear analysis of plate and shell structures, Computational Mechanics 35 (1) (2004) 72–84. doi:10.1007/s00466-004-0605-x.

[14] K. Sze, W. Chan, T. Pian, An eight-node hybrid-stress solid-shell element for geometric non-linear analysis of elastic shells, International

Journal for Numerical Methods in Engineering 55 (7) (2002) 853–878. doi:10.1002/nme.535.

[15] S. Klinkel, F. Gruttmann, W. Wagner, A robust non-linear solid shell element based on a mixed variational formulation, Computer Methods in Applied Mechanics and Engineering 195 (1-3) (2006) 179–201. doi:10.1016/j.cma.2005.01.013.

[16] G. Garcea, G. Trunfio, R. Casciaro, Mixed formulation and locking in path-following nonlinear analysis, Computer Methods in Applied Mechanics and Engineering 165 (1-4) (1998) 247–272.

[17] G. Garcea, G. Salerno, R. Casciaro, Extrapolation locking and its sanitization in Koiter's asymptotic analysis, Computer Methods in Applied Mechanics and Engineering 180 (1-2) (1999) 137–167.

[18] G. Garcea, Mixed formulation in Koiter analysis of thin-walled beams, Computer Methods in Applied Mechanics and Engineering 190 (26-27) (2001) 3369–3399.

[19] G. Garcea, G. A. Trunfio, R. Casciaro, Path-following analysis of thin-walled structures and comparison with asymptotic post-critical solutions, International Journal for Numerical Methods in Engineering 55 (1) (2002) 73–100.

[20] D. S. Simulia, ABAQUS 6.12/Analysis User's Manual. Volume IV: Elements, Dassault Systèmes Simulia, USA, 2012.

[21] D. Magisano, L. Leonetti, G. Garcea, Advantages of the mixed format in geometrically nonlinear analysis of beams and shells using solid finite elements, International Journal for Numerical Methods in Engineering (2016) n/a–n/aNme.5322. doi:10.1002/nme.5322.
URL http://dx.doi.org/10.1002/nme.5322

[22] E. Riks, An incremental approach to the solution of snapping and buckling problems, International Journal of Solids and Structures 15 (7) (1979) 529–551. doi:10.1016/0020-7683(79)90081-7.

[23] P.-A. Ubach, E. Oñate, New rotation-free finite element shell triangle accurately using geometrical data, Computer Methods in Applied Mechanics and Engineering 199 (5-8) (2010) 383–391. doi:10.1016/j.cma.2009.01.006.

[24] H.-M. Jeon, Y. Lee, P.-S. Lee, K.-J. Bathe, The mitc3+ shell element in geometric nonlinear analysis, Computers and Structures 146 (2015) 91–104. doi:10.1016/j.compstruc.2014.09.004.

[25] M. Schwarze, S. Reese, A reduced integration solid-shell finite element based on the eas and the ans concept-large deformation problems, International Journal for Numerical Methods in Engineering 85 (3) (2011) 289–329. doi:10.1002/nme.2966.

[26] Q. Li, Y. Liu, Z. Zhang, W. Zhong, A new reduced integration solid-shell element based on EAS and ANS with hourglass stabilization, International Journal for Numerical Methods in Engineering (2015) 1885–1891arXiv:1010.1724, doi:10.1002/nme.

[27] M. Bischoff, E. Ramm, Shear deformable shell elements for large strains and rotations, International Journal for Numerical Methods in Engineering 40 (23) (1997) 4427–4449.

[28] K. Sze, A. Ghali, Hybrid hexahedral element for solids, plates, shells and beams by selective scaling, International Journal for Numerical Methods in Engineering 36 (9) (1993) 1519–1540.

[29] L. Vu-Quoc, X. G. Tan, Optimal solid shells for non-linear analyses of multilayer composites. I Statics, Computer Methods in Applied Mechanics and Engineering 192 (9-10) (2003) 975–1016. doi:10.1016/S0045-7825(02)00435-8.

[30] K. Liang, M. Ruess, M. Abdalla, Co-rotational finite element formulation used in the koiter-newton method for nonlinear buckling analyses, Finite Elements in Analysis and Designdoi:10.1016/j.finel.2016.03.006.

[31] C. Sansour, F. Kollmann, Families of 4-node and 9-node finite elements for a finite deformation shell theory. an assessment of hybrid stress, hybrid strain and enhanced strain elements, Computational Mechanics 24 (6) (2000) 435–447. doi:10.1007/s004660050003.

[32] G. Zagari, A. Madeo, R. Casciaro, S. De Miranda, F. Ubertini, Koiter analysis of folded structures using a corotational approach, International Journal of Solids and Structures 50 (5) (2013) 755–765. doi:10.1016/j.ijsolstr.2012.11.007.

[33] E. Lindgaard, E. Lund, Nonlinear buckling optimization of composite structures, Computer Methods in Applied Mechanics and Engineering 199 (37-40) (2010) 2319–2330. doi:10.1016/j.cma.2010.02.005.

[34] T. Hughes, J. Cottrell, Y. Bazilevs, Isogeometric analysis: Cad, finite elements, nurbs, exact geometry and mesh refinement, Computer Methods in Applied Mechanics and Engineering 194 (39-41) (2005) 4135–4195. doi:10.1016/j.cma.2004.10.008.

[35] K. Liang, M. Ruess, M. Abdalla, The Koiter-Newton approach using von Karman kinematics for buckling analyses of imperfection sensitive structures, Computer Methods in Applied Mechanics and Engineering 279 (2014) 440–468. doi:10.1016/j.cma.2014.07.008.

[36] K. Liang, M. Abdalla, Z. Gürdal, A Koiter-Newton approach for nonlinear structural analysis, International Journal for Numerical Methods in Engineering 96 (12) (2013) 763–786. doi:10.1002/nme.4581.